INTERNATIONAL JOURNAL OF INTEGRATED ENGINEERING
ISSN: 2229-838X e-ISSN: 2600-7916

IJIE

Vol. 17 No. 8 (2025) 227-243
https://publisher.uthm.edu.my/ojs/index.php/ijie

An Optimization Approach and Environmental Evaluation of Aluminium AA7075 Alloy in Metal Forming Process by Solid State Recycling Hot Press Forging

Ikhwan Shah Tisadi Tukiat[1], Nur Kamilah Yusuf[1]*, Mohd Amri Lajis[1], Muhamad Haikal Mohd Khaireez[1]

[1] *Sustainable Manufacturing and Recycling Technology (SMART), Advanced Manufacturing and Material Center (AMMC), Institute for Integrated Engineering (I^2E), Universiti Tun Hussein Onn Malaysia (UTHM), 86400, Parit Raja, Johor, MALAYSIA*

*Corresponding Author: nurkamilah@uthm.edu.my
DOI: https://doi.org/10.30880/ijie.2025.17.08.020

Article Info

Received: 20 June 2025
Accepted: 30 November 2025
Available online: 31 December 2025

Keywords

Solid-state recycling (SSR); conventional recycling (CR); direct recycling hot press forging (DRHPF); response surface methodology (RSM); life cycle assessment (LCA)

Abstract

This study presents the optimization of Direct Recycling Hot Press Forging (DR-HPF) parameters for AA7075 aluminium alloy to enhance mechanical properties and minimize environmental impact. Response Surface Methodology (RSM) with Central Composite Design (CCD) was used to investigate the effects of forging temperature and soaking time on ultimate tensile strength (UTS), elongation to failure (ETF), and global warming potential (GWP). The optimized DR-HPF process, conducted at 480°C and 86 minutes soaking time, achieved a maximum UTS of approximately 251.33 MPa and an ETF of 6.9%, marking significant improvements over conventional recycling methods. Life Cycle Assessment showed a reduction of global warming potential by more than 85% and energy consumption by approximately 69% compared to remelting processes. This work uniquely integrates process optimization and detailed environmental evaluation, advancing sustainable recycling practices for high-performance aluminium alloys.

1. Introduction

Aluminium is integral to diverse industries including automotive and aerospace due to its advantageous properties such as high strength-to-weight ratio and corrosion resistance. However, conventional primary aluminium production is energy-intensive with significant environmental impacts, which has prompted increasing adoption of aluminium recycling to mitigate resource depletion and reduce carbon footprints [1], [2], [3], [4], [5], [6], [7].Solid-state recycling (SSR) of aluminium alloys has emerged as a promising alternative to conventional melting-based recycling, offering benefits like reduced energy consumption, minimized metal loss, and superior material properties due to the absence of melting [8], [9], [10], [11], [12], [13], [14], [15], [16], [17]. Among SSR techniques, methods such as friction stir extrusion and spark plasma sintering (SPS) have demonstrated potential for consolidating aluminum scrap. Friction stir extrusion uses severe plastic deformation to achieve bonding but requires complex tooling and process control, while SPS employs electrical currents and plasma generation to sinter chips, involving intricate equipment and significant operational complexity [11], [15], [16].

In contrast, Direct Recycling Hot Press Forging (DR-HPF) presents a meltless, simpler, and energy-efficient approach that consolidates aluminium alloy chips through controlled temperature and pressure without the complexities of specialized electrical setups. DR-HPF can reduce environmental impacts substantially, achieving

up to 69% reduction in global warming potential compared to conventional recycling practices, by eliminating melting losses and lowering energy requirements [11], [18]. Despite these advantages, few studies have systematically optimized DR-HPF process parameters for key alloys like AA7075, which is widely used in high-performance applications and demands precise control over mechanical properties.

Previous SSR research has extensively examined individual process methods and mechanical outcomes but often lacks integrated optimization strategies and environmental evaluations. Optimization techniques such as Taguchi methods, artificial neural networks, and Response Surface Methodology (RSM) have been applied in alloy recycling; however, their application to DR-HPF specifically for AA7075 remains limited [19], [20], [21], [22], [23], [24], [25], [26], [27], [28], [29], [30], [31]. Furthermore, environmental assessments focusing on energy use and global warming potential are critical to validate the sustainability claims of emerging SSR technologies.

This study addresses these gaps by applying RSM coupled with Central Composite Design (CCD) to optimize operating temperature and soaking time in the DR-HPF process for AA7075 alloy. The research aims to simultaneously enhance mechanical properties—specifically ultimate tensile strength (UTS) and elongation to failure (ETF)—and assess the environmental impact through comprehensive Life Cycle Assessment (LCA). By integrating process parameter optimization with environmental evaluation, this work contributes novel insights towards sustainable and high-performance aluminium recycling methods.

Nomenclature is included if necessary	
CCD	Central Composite Design
CR	conventional recycling
DF	Desirability Function
DOE	Design of Experiments
DRHPF	direct recycling hot press forging
ETF	Elongation to Failure
GWP	global warming potential
LCA	life cycle assessment
SSR	solid-state recycling
RSM	response surface methodology
UTS	Ultimate Tensile Strength

2. Materials and Methods

2.1 Direct Recycling Hot Press Forging (DR-HPF)

The recycled AA7075 chips used in this study had an average particle size ranging from approximately 1 to 3 mm, consistent with previous works [31], [32], [33]. These chips were cleaned using an ultrasonic bath (Elmasonic S 60 H) in a 99.5% pure acetone solution to remove contaminants that could interfere with bonding during processing. After cleaning, the chips were dried in a thermal oven (SOV140B) at 60°C for 30 minutes to ensure complete evaporation of residual solvents. Ensuring the chips were free of impurities was critical to maintain the chemical integrity of the material throughout the process.

For consolidation, 12 grams of the cleaned AA7075 chips were loaded into a close-die steel mold shaped like a dog bone. The mold was then subjected to a pre-compaction cycle repeated four times at a constant pressure of 350 kN using the Hot Press Forging (HPF) machine. Figure 1 presents a schematic overview of the entire Direct Recycling Hot Press Forging (DR-HPF) process, integrating initial compaction, heating, soaking, and forging stages. The mold was heated to the target forging temperatures — 380, 430, and 480°C — and maintained for soaking times of 0, 60, or 120 minutes to ensure uniform temperature distribution throughout the specimen before forging [31].

Int. Journal of Integrated Engineering Vol. 17 No. 8 (2025) p. 227-243

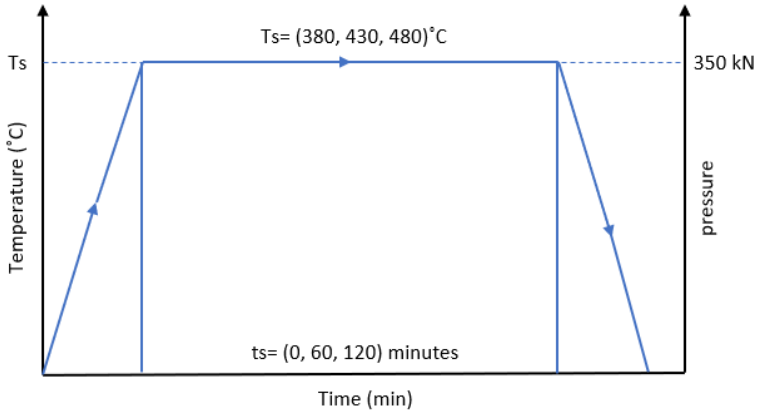

Fig. 1 *The DR-HPF process diagram*

The selection of these specific temperature and soaking time ranges was guided by a review of the literature and industrial standards for AA7075 processing, including guidelines from the ASM Aerospace Specification Metal data ASM International, 2020 [34], [35]. Recommended forging temperatures for AA7075 and similar aluminum alloys typically range between 380 and 440°C, which facilitates optimal material flow without melting [36]. For solution heat treatment, temperatures between 450 and 540°C are common, with 480°C the typical target, corresponding closely to the solidus temperature around 477°C [37]. Soaking times reported in previous studies vary widely from 10 to 480 minutes, with 60 minutes frequently chosen to balance homogenization and processing efficiency [38].

Table 1 *The operating parameters for the HPF process by previous studies on AA7075 Aluminium alloys*

No	Details		Solution heat treatment (SHT)	
	Author	Year	Operating Temperature (°C)	Holding time (minutes)
2	Hayat	2012	480	-
8	Lin et al.	2013	470	60
9	Canakci &Varol	2014	500	60
10	Ibrahim et al.	2014	470	480
11	Rometsch et al.	2014	480	30-60
12	Joshi et al.	2015	540	-
13	W.Guo et al.	2015	490	90
14	Gholami et al.	2015	480	240
15	Shaeri et al.	2015	470	60
16	Park & Kim	2016	450	-
17	Veeravalli et al.	2016	450	120
18	Aoba et al.	2017	490	60
24	Jung et al.	2018	480	30
29	Kumar et al.	2018	470	60
30	Ku et al.	2018	490	60
31	Araoyinbo et al.	2018	470	60
32	Darsano et al.	2018	500	129
33	Kong et al.	2018	480	10
34	Wei et al.	2018	466	60
35	Pankade et al.	2018	460	60
36	Wang et al.	2018	475	60
37	Niu et al.	2019	490	90
38	Sun et al.	2019	470	60
39	Zhang et al.	2019	480	60
40	Sajadifar et al.	2019	480	60

No	Details		Solution heat treatment (SHT)	
	Author	Year	Operating Temperature (°C)	Holding time (minutes)
41	Pankade et al.	2019	480	60
42	Z.Zhang et al.	2019	475	20
43	Bakkiyaraj et al.	2020	500	60
44	Wang et al.	2020	475	60
45	Scharifi et al.	2021	480	15
46	Abdelfatah et al.	2021	470	60
47	Vikas ey al.	2021	400	60
48	Graf et al.	2022	500	20
49	Kalsar et al.	2022	465	40
50	Watzl et al.	2022	480	15
51	Abolhasani et al.	2022	470	10
52	Min et al.	2022	470	60
53	Kumar et al.	2022	480	60
54	Qi et al.	2023	470	120
55	Tai et al.	2023	490	30
56	Scharifi et al.	2023	480	15
57	Feng et al.	2023	475	35
58	Yang et al.	2023	480	180
59	Ma et al. (a)	2023	480	90
60	Ma et al. (b)	2023	480	60
61	Chen et al.	2024	470	120
62	Gu et al.	2024	475	35
63	Lahbari et al.	2024	515	26
64	Mukherjee et al.	2024	470	60

2.2 Response Surface Methodology (RSM)

This study uses RSM to analyze the relationship between three measured responses: Ultimate Tensile Strength (UTS), Elongation to Failure (ETF), and Global Warming Potential (GWP), and two significant parameters: operating temperature and soaking time. Replicated experiments were conducted at the design center to assess measurement error, following randomized order protocols common in design systems. Coded variables were utilized for their dimensionless nature, enabling evaluation of the impact of changes in each design factor over a one-unit interval. Coded designs were directly compared to model coefficients and the relationship is bound as in Equation 1 [39].

$$C = \frac{X - \frac{(A_l + A_h)}{2}}{\frac{(A_h - A_l)}{2}} \quad (1)$$

Where C is known as the coded design variable, meanwhile X is the actual intended magnitude, and A_l and A_h are respectively the actual low and high magnitude. The ideal model for predicting optimal conditions was a quadratic model, expressed as Equation 2 [40], where y represents the measured response, x_i and x_j denote input factors, β_0 is a constant coefficient, β_j, β_{jj} and β_{ij} represent linear, quadratic, and second-order interaction coefficients respectively, k is the number of analyzed factors, and ϵ represents error. The fitted polynomial condition was visualized using surface and contour plots to understand the connection between responses and experimental levels of each factor. Model equation adequacy for predicting optimum reaction values was validated using experimental outcomes [39], [41], [42].

Int. Journal of Integrated Engineering Vol. 17 No. 8 (2025) p. 227-243

$$y = \beta_0 + \sum_{j=1}^{k} \beta_j x_j + \sum_{j=1}^{k} \beta_{jj} x^2{}_j + \sum_{i} \sum_{<j=1}^{k} \beta_{ij} x_i x_j + \epsilon \quad (2)$$

The Analysis of Variance (ANOVA) was implemented in the model to assess significance. A model was considered significant if the p-value was less than 0.05. Key indicators such as R2 and adjusted R2 values were used to evaluate model significance. The predicted R2 was considered in fair agreement with the adjusted R2 when the difference was less than 0.2 [43].

$$D = (d_1 \times d_2 \times \ldots \times d_n)^{\frac{1}{n}} = \left[\prod_{i=1}^{n} d_i\right]^{\frac{1}{n}} \quad (3)$$

The Desirability Function (DF) approach was employed for optimization, offering a single dimensionless measure of combined responses. The DF ranged from zero outside cutoff points to one for the objective, allowing for adjustments in weight or significance to optimize objectives. Equation 3 represents the combined DF, with *D* as the overall desirability and n as the number of measured responses. Recommendations from Derringer et al. [44] were considered for varying desirability functions depending on whether a specific response y was to be minimized, maximized, or targeted.

2.3 Experimental Design

The HPF process employed the CCD, which is a full factorial design, with all possible combinations of a factor variable having two levels. The star points are situated on the face of the design's cube part. The points represented the α-value of 1 (face-centred). The centre points were at the midpoint of each factor's range, with all levels set to coded level 0, and were repeated twice. Two factors were evaluated in this study, and their low and high levels (as determined by Equation (1)) are shown in Table 2.

Table 2 *Factor variables and levels for the measured response surface study*

Factors	Unit	Notation	Levels		
			(-1)	(0)	(+1)
Operating Temperature	˚C	A	380	430	480
Soaking Time	minutes	B	0	60	120

The measured responses were UTS, ETF, and GWP. Based on the above information, the software produced a finished design layout that showed the actual midpoint values to be used, which were 430°C for temperature and 60 minutes for soaking time. Table 3 shows the result of the DR-HPF performed according to the experimental plan. The input results were further analysed using Design Expert 13 software. In short, a review of the fit summary for the measured responses revealed that the quadratic model was statistically significant, hence it was used for further analysis.

Table 3 *The response surface study result*

Run	Coded Factor		Actual Factor		Responses		
	C1	C2	A (˚C)	B (Min)	UTS (MPa)	ETF (%)	GWP ($kgCO_2$-eq/kg)
1	+1	0	480	60	218.87	4.68	17.30
2	+1	-1	480	0	185.89	2.3	6.56
3	0	+1	430	120	113.08	1.28	24.99
4	0	0	430	60	90.83	0.78	15.39
5	0	0	430	60	70.73	1.01	15.36
6	0	0	430	60	77.85	1.05	15.58
7	0	-1	430	0	63.19	0.64	4.58
8	+1	+1	480	120	245.62	6.91	26.73
9	-1	+1	380	120	43.48	0.87	24.05
10	-1	-1	380	0	17.02	0.53	3.96
11	-1	0	380	60	26.48	0.79	14.44

2.4 Life Cycle Assessment (LCA)

LCA is a widely accepted methodology for quantifying the environmental impacts associated with products or systems throughout their life cycles. In this study, the system boundary is defined around the production of aluminum scrap, encompassing primary outputs and related by-product streams, as illustrated in Figure 2. To provide a comprehensive environmental evaluation, a comparative LCA is performed between the DR-HPF process and the Conventional Recycling (CR) method, both commencing from identical aluminum scrap feedstock. This comparison evaluates not only technical feasibility but also potential energy and material savings associated with each recycling pathway.

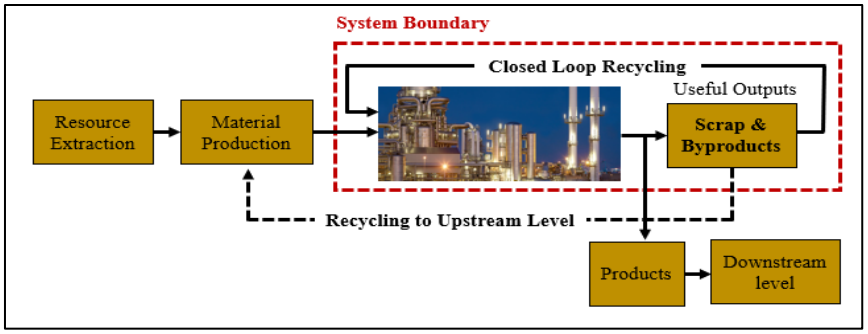

Fig. 2 *The system boundary and useful outputs*

Figure 3 offers a detailed visualization of the LCA outcomes for both recycling routes, enabling a more precise environmental impact assessment compared to preliminary estimates. The background data and process inventories for the LCA modeling were compiled using SimaPro 9.6 software, in alignment with the ISO 14040 and ISO 14044 international standards for life cycle assessment [45], [46].

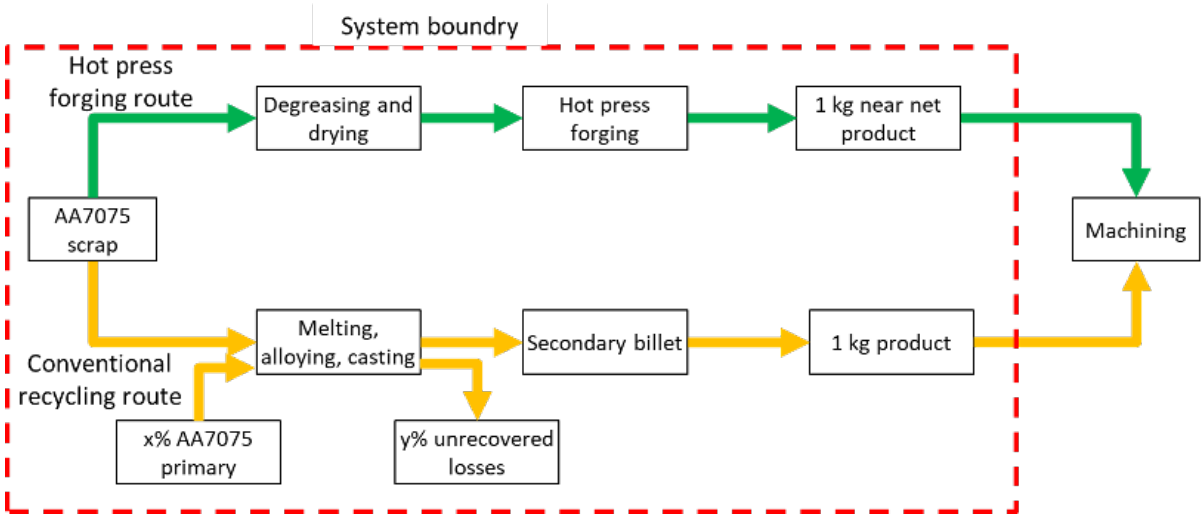

Fig. 3 *The system boundary for DR-HPF and CR pathways*

Data representing the CR route were primarily obtained from the Ecoinvent database version 3.8 and supplemented with pertinent published literature to reflect industry-standard values. In contrast, data specific to the DR-HPF process were generated through in-house analyses conducted at Universiti Tun Hussein Onn Malaysia (UTHM), ensuring tailored and recent inventory inputs reflective of the novel process.

Table 4 details the primary life cycle inventory (LCI) data for materials and process inputs, alongside their respective data sources. Environmental impacts were assessed using the ReCiPe 2016 impact assessment method incorporating both midpoint and endpoint indicators [47]. The hierarchy perspective with a 100-year time horizon was adopted as the default approach, providing balanced weighting of environmental effect categories relevant to sustainable material processing.

Int. Journal of Integrated Engineering Vol. 17 No. 8 (2025) p. 227-243

Table 4 *The details of the main life cycle inventory (LCI) and sources*

Route	Process	Detail	Source
DR-HPF (optimal value)	Chemical degreasing and drying	This dataset includes the energy consumption and operating materials required to run degreasing baths	Ecoinvent database version 3.11 (2025)
	Optimum parameter for DR-HPF	Heating at 480°C for 86 minutes 350kN constant force	Energy consumption was measured per unit of mass
CR (remelting)	Secondary production of aluminium (new scrap)	Melting, casting and aluminium dross recycling are included. The loss of Mg is also included.	Ecoinvent database version 3.11 (2025)
	Primary AA7075	The concentration of an alloying element in the middle of the alloy tolerance limits.	Ecoinvent database version 3.11 (2025)
	Electricity	Medium voltage is provided for the aluminium industry in Malaysia	Ecoinvent database version 3.11 (2025)

The total power consumption is given in Equation 4 [48], [49] below:

$$P = \frac{\sqrt{3}\ x\ PF\ x\ I\ x\ V}{1000} \tag{4}$$

Where P is the Power in kilowatts (kW), PF is a constant Power Factor of 0.8, I is current in ampere (A), and V is the voltage in volts (V). Additionally, the equation contributes to understanding the sustainability and efficiency of the recycling pathways under consideration.
The impact assessment is conducted using the ReCiPe method, which provides indicator scores representing the severity of environmental effect categories. Both midpoint and endpoint indicators are employed, following a hierarchist perspective for a 100-year duration as the default approach.

3. Results and Analysis

3.1 Response Surface Methodology

3.1.1 Analysis of UTS

To validate the regression model's adequacy, tests of significance were conducted for the overall model, individual coefficients, and lack of fit. Table 5 summarizes the Analysis of Variance (ANOVA) results for the quadratic model predicting Ultimate Tensile Strength (UTS). The model's F-value of 216.98 indicates high significance, with only a 0.01% probability that such a large value could arise from random noise. Terms with p-values below 0.05 were considered significant contributors to the model. Specifically, operating temperature (A), soaking time (B), and the quadratic term for temperature (A^2) were significant, while other terms were not. Insignificant terms can be excluded to improve model parsimony, except those required to maintain hierarchy.

The Lack of Fit F-value of 0.23 suggests an 87.01% chance that the observed lack of fit could be attributed to random error, indicating the model fits well—a desirable outcome.

A refined quadratic model was developed by removing non-significant terms through a backward elimination approach. The ANOVA for this reduced model (Table 5) shows an improved F-value of 234.86 and a Lack of Fit F-value of 0.75, with a 65.51% probability that any observed lack of fit is due to noise, maintaining its insignificance.

Key model quality metrics further support the model's strength. The coefficient of determination, R^2, is 0.9954, indicating that 99.54% of the variance in UTS is explained by the model. The adjusted R^2 of 0.9902 and predicted R^2 of 0.9721 are in reasonable agreement, confirming strong predictive capability without overfitting. All significant terms in the reduced model—operating temperature (A), soaking time (B), and temperature squared (A^2)—were retained based on statistical merit.

Overall, these statistics confirm that the quadratic regression model is highly significant and reliable for forecasting UTS under the studied conditions [19]. The final quadratic model equation in terms of coded factors for UTS after pooling is expressed below:

$$UTS = +83.14 + 93.9A + 22.68B + 39.76A^2 \tag{5}$$

Table 5 *A reduced quadratic model of ANOVA for UTS before and after pooling*

Source	Before pooling						After pooling					
	Sum of Square	df	Mean Square	F-value	p-value		Sum of Square	df	Mean Square	F-value	p-value	
Model	60620.11	5	12124.02	216.98	<0.0001	Significant	60300.41	3	20100.14	234.9	<0.0001	Significant
A – operating temperature	52903.26	1	52903.26	946.79	<0.0001		52903.26	1	52903.26	618.2	<0.0001	
B – soaking time	3086.29	1	3086.29	55.23	0.0007		3086.29	1	3086.29	36.06	0.0005	
AB	276.72	1	276.72	4.95	0.0766							
A^2	3786.1	1	3786.1	67.76	0.0004		4310.85	1	4310.85	50.37	0.0002	
B^2	42.98	1	42.98	0.7692	0.4206							
Residual	279.38	5	55.88				599.09	7	85.58			
Lack of Fit	71.65	3	23.88	0.23	0.8701	Not Significant	391.36	5	78.27	0.754	0.6551	Not Significant
Pure Error	207.73	2	103.86				207.73	2	103.86			
Cor Total	60899.49	#					60899.49	10				
Std. Dev	7.48		R^2		0.9954		9.25		R^2		0.9902	
Mean	104.82		Adjusted R^2		0.9908		104.82		Adjusted R^2		0.9859	
C.V %	7.13		Predicted R^2		0.9838		8.83		Predicted R^2		0.9721	
			Adequate Precision		42.2337				Adequate Precision		41.795	

Figure 4 displays the effect of operating temperature and soaking time for UTS on a 3D surface graphic. It was observed that temperature (A) had a greater effect on soaking time (B) to produce a better result on UTS. Apparently, the UTS increased as the operating temperature and soaking time rose. The UTS could be improved by raising the operating temperature and then the soaking time.

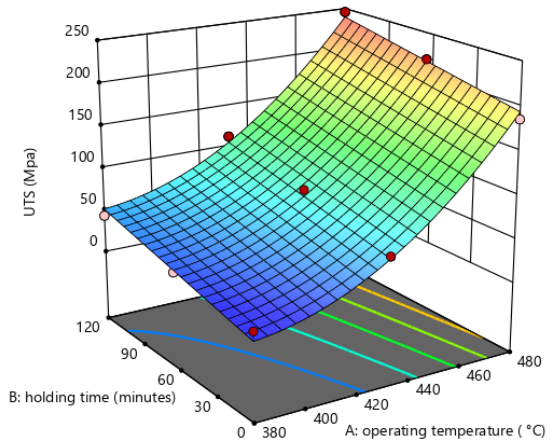

Fig. 4 *Effect of factors A (operating temperature) and B (soaking time) on UTS*

3.1.2 Analysis of ETF

The analysis of Elongation to Failure (ETF) focused on optimizing this mechanical property response. As presented in Table 6, the initial quadratic ANOVA model for ETF before pooling demonstrated a strong correlation between independent variables and ETF, with an R^2 of 97.19% and an adjusted R^2 of 94.38%. The model was statistically significant (p-value < 0.05) and exhibited an insignificant Lack of Fit, indicating an adequate fit.
Significant model terms included the main effects of operating temperature (A) and soaking time (B), their interaction (AB), and the second-order term of operating temperature (A^2). However, the predicted R^2 was only 71%, revealing a notable 25% gap from the adjusted R^2. This discrepancy suggests that the model may have

Int. Journal of Integrated Engineering Vol. 17 No. 8 (2025) p. 227-243

limitations in predicting ETF accurately for new, unseen data, implying the need for potential refinement or alternative modeling approaches to better capture the underlying complexities influencing ETF.

To address this, the model underwent backward elimination to remove non-significant terms, leading to a reduced quadratic model detailed in Table 6. The reduced model yielded an F-value of 51.82, affirming statistical significance with only a 0.01% likelihood of this result arising by chance. Significant terms remained consistent: operating temperature (A), soaking time (B), their interaction (AB), and the quadratic term (A^2).The Lack of Fit F-value in the reduced model was 13.29, corresponding to a 7.12% probability that this lack of fit could be due to noise. Since this is above the 5% threshold, the Lack of Fit remains statistically insignificant—an indication of a well-fitting model.

The refined model's predicted R^2 improved to 80.88%, with strong agreement to the adjusted R^2 of 95.31%, indicating better predictive reliability. The coefficient of determination, R^2, remained high at 97.19%, suggesting the model explains the majority of variation in ETF. Additionally, the signal-to-noise metric, Adequate Precision, exceeded the desirable threshold of 4, highlighting an adequate signal for reliable model predictions.

Table 6 *ANOVA reduced quadratic model for ETF before and after pooling*

	Before pooling						After pooling					
Source	Sum of Square	df	Mean Square	F-value	p-value		Sum of Square	df	Mean Square	F-value	p-value	
Model	40.45	5	8.09	34.59	0.0007	Significant	40.45	4	10.11	51.82	<0.0001	Significant
A – operating temperature	22.62	1	22.62	96.71	0.0002		22.62	1	22.62	115.9	<0.0001	
B – soaking time	5.21	1	5.21	22.27	0.0052		5.21	1	5.21	26.69	0.0021	
AB	4.56	1	4.56	19.49	0.0069		4.56	1	4.56	23.36	0.0029	
A^2	7.55	1	7.55	32.27	0.0024		8.07	1	8.07	41.33	0.0007	
B^2	0.0015	1	0.0015	0.0062	0.9402							
Residual	1.17	5	0.233				1.17	6	0.1952			
Lack of Fit	1.13	3	0.3757	17.69	0.054	Not Significant	1.13	4	0.2821	13.29	0.0721	Not Significant
Pure Error	0.0425	2	0.0212				0.0425	2	0.0212			
Cor Total	41.61	#					41.62	10				
Std. Dev	0.4836		R^2		0.9719		0.4418		R^2		0.9719	
Mean	1.89		Adjusted R^2		0.9438		1.89		Adjusted R^2		0.9531	
C.V %	25.59		Predicted R^2		0.7112		23.37		Predicted R^2		0.8088	
			Adequate Precision		18.4741				Adequate Precision		22.1337	

The final quadratic model equation in terms of coded factors for ETF after pooling is expressed below:

$$ETF = +0.952 + 1.94A + 0.9317B + 1.07AB + 1.72A^2 \quad (6)$$

The 3D surface of the ETF graphic image is shown in Figure 5. The operating temperature (effect factor A) predominated over the soaking time (effect factor B). Similarly, the ETF tended to increase significantly when the temperature rose from 380°C to 480°C. Likewise, the increase in soaking time from 0 to 120 minutes enhanced the variation of the ETF. Thus, maximal ETF was attained at the maximum operating forging temperature of 480°C and maximum soaking time of 120 minutes.

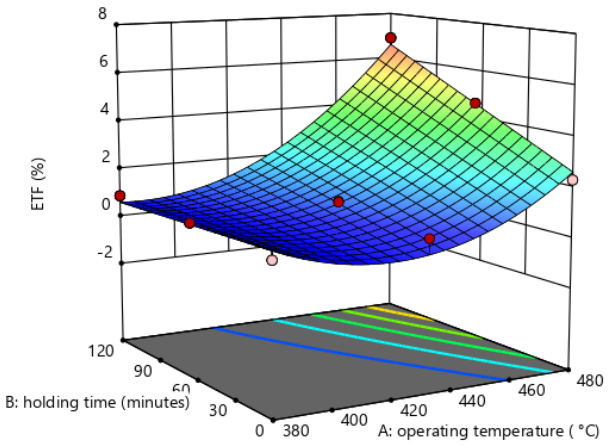

Fig. 5 *Effect of Factor A (operating temperature and B (soaking time) on ETF*

3.1.3 Analysis of GWP

As previously stated, tests of significance for the regression model, individual coefficients, and lack of fit were conducted to validate the GWP quadratic model. Table 7 presents the ANOVA results for the full quadratic model before pooling. The model's F-value of 7,936.00 indicates strong significance, with only a 0.01% chance that such a large F-value could be due to random noise. P-values less than 0.05 confirmed that key model terms were significant. Specifically, operating temperature (A), soaking time (B), and their second-order terms (A^2 and B^2) were significant, while other terms were not.

The Lack of Fit F-value was 1.18, indicating that lack of fit was not statistically significant compared to pure error, with a 48.93% probability that such a value could arise from noise. This confirms the model fits the data well. Moreover, the predicted R^2 of 0.9991 was in close agreement with the adjusted R^2 of 0.9997, underscoring strong predictive capability of the model.

After removing non-significant terms via pooling, the reduced quadratic model's ANOVA is also shown in Table 7. This refined model demonstrated an even higher F-value of 11,667.21, again highly significant with only a 0.01% probability of occurring by chance. Significant terms remained operating temperature (A), soaking time (B), and their second-order effects (A^2 and B^2). Terms with P-values above 0.10 were removed as non-significant.

The Lack of Fit for the reduced model was 0.91, corresponding to a 58.25% chance that any lack of fit is due to noise, confirming model adequacy. The predicted R^2 improved slightly to 0.9996 and remained consistent with an adjusted R^2 of 0.9998. The coefficient of determination, R^2, was 0.9999—almost perfect fit, indicating the model explains nearly all variability in GWP.

Int. Journal of Integrated Engineering Vol. 17 No. 8 (2025) p. 227-243

Table 7 *ANOVA reduced quadratic model for GWP before and after pooling*

	Before pooling						After pooling					
Source	Sum of Square	df	Mean Square	F-value	p-value		Sum of Square	df	Mean Square	F-value	p-value	
Model	625.72	5	125.14	7936	<0.0001	Significant	625.72	4	156.43	11667	<0.0001	Significant
A – operating temperature	11.04	1	11.04	700.31	<0.0001		11.04	1	11.04	823.7	<0.0001	
B – soaking time	613.47	1	613.47	38904	<0.0001		613.47	1	613.47	45756	<0.0001	
AB	0.0016	1	0.0016	0.1015	0.763							
A^2	0.5991	1	0.5991	37.99	0.0016		0.5991	1	0.5991	44.69	0.0005	
B^2	0.908	1	0.908	57.58	0.0006		0.908	1	0.908	67.72	0.0002	
Residual	0.0788	5	0.0158				0.0804	6	0.0134			
Lack of Fit	0.0504	3	0.0168	1.18	0.4893	Not Significant	0.052	4	0.013	0.913	0.5825	Not Significant
Pure Error	0.0285	2	0.0142				0.0285	2	0.0142			
Cor Total	625.8	#					625.8	10				
Std. Dev	0.1256		R^2		0.9999		0.158		R^2		0.9999	
Mean	15.36		Adjusted R^2		0.9997		15.36		Adjusted R^2		0.9998	
C.V %	0.8176		Predicted R^2		0.9991		0.7539		Predicted R^2		0.9996	
			Adequate Precision		247.313				Adequate Precision		293.81	

The final quadratic model equation in terms of coded factors for GWP after pooling is expressed below:

$$GWP = +15.42 + 1.36A + 10.11B + 0.4863A^2 + 0.5987B^2 \quad (7)$$

The 3D surface graphic for GWP is shown in Figure 6. The soaking time (factor B) showed dominance rather than the operating temperature (factor A). The variation in the GWP grew as the holding time (factor B) rose from 0 to 120 minutes. In addition, the GWP tended to increase with an increase in temperature (factor A) from 380°C to 480°C. Hence, the maximum GWP was obtained at the maximum soaking time (120 min) and maximum operating temperature (480°C). The importance of minimizing GWP is essential for mitigating climate change and crucial for environmental sustainability.

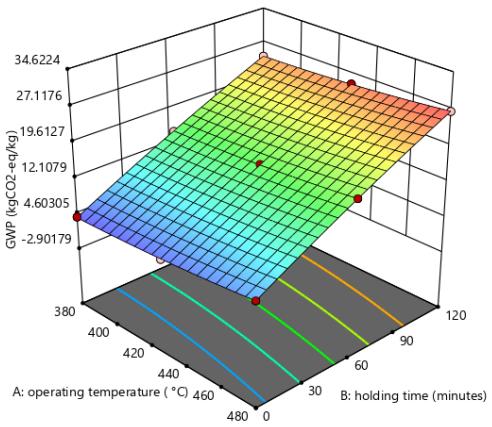

Fig. 6 *Effect of factors A (operating temperature) and B (soaking time) on GWP*

3.1.4 Optimization Desirability

This study aimed to maximize Ultimate Tensile Strength (UTS), targeting 228 MPa, and Elongation to Failure (ETF), while simultaneously minimizing the Global Warming Potential (GWP) to benefit the environment. Table 8 presents the optimal process parameters derived through desirability analysis—maximizing UTS and ETF, and minimizing GWP. The optimal conditions identified were an operating temperature of 480°C combined with 86 minutes of soaking time, yielding a desirability score of 78%. Under these conditions, the predicted UTS was 228 MPa, ETF was 5.48%, and GWP was 21.47 kg CO_2-equivalent per kilogram of material.

Table 8 *Suggested parameter for the optimal output*

Solution	Temp.	Soaking time	UTS	ETF	GWP	Desirability	
1	480	86	228.000	5.477	21.470	0.780	**Selected**
2	480	78	223.930	5.239	20.310	0.773	

Unlike earlier studies that optimized individual responses separately, this work used overlay contour plots in the response surface methodology (RSM) to identify a feasible region simultaneously satisfying all target responses [31], [50]. The overlay plot for GWP, UTS, and ETF clearly delineates areas meeting the criteria—yellow zones represent the feasible operating window, while shaded areas do not satisfy all response targets. This multi-response optimization approach offers a more holistic view of process trade-offs and synergies, guiding decision-making toward balanced performance [39].

To verify the predictive capability of the RSM quadratic models, confirmatory experiments were performed within the established factor ranges. Two validation runs, summarized in Table 9, compared predicted values with actual experimental results for UTS, ETF, and GWP. Errors between predicted and observed values ranged from 3.27% to 10.23% for UTS, 9.85% to 23.91% for ETF, and a notably low 0.33% to 0.56% for GWP. While ETF errors were relatively high, all results remained within the 95% confidence intervals, confirming the models' robustness and reproducibility. This validation supports the empirical models as reliable tools for forecasting and optimizing DR-HPF process outcomes.

Table 9 *Confirmation run with an estimated value*

Responses	Details	Confirmation test	
		1	2
	Operating temperature, ˚C	480	480
	Soaking time, min	86	86
Ultimate Tensile Strength, UTS (MPa)	Experimental	235.46	251.33
	Estimation	228.00	228.00
	Error (%)	3.27	10.23
Elongation to Failure, ETF (%)	Experimental	6.02	6.79
	Estimation	5.48	5.48
	Error (%)	9.85	23.91
Global Warming Potential, GWP (kg CO_2-eq/kg)	Experimental	21.59	21.54
	Estimation	21.47	21.47
	Error (%)	0.56	0.33

This study effectively linked physicochemical parameters—primarily forging temperature and soaking time—with mechanical performance and environmental impact. Using RSM allowed deep insight into how these factors influence key responses like UTS, ETF, and GWP. The findings highlight the critical role of processing conditions in shaping material properties and environmental sustainability, emphasizing the value of integrated optimization in metallurgical recycling processes [33].

3.1.5 Effect of the Parameters

This study explores how forging temperature and holding time influence the mechanical and physicochemical properties of the alloy. Results show that increasing forging temperature from 380°C to 480°C significantly boosts both ultimate tensile strength (UTS) and elongation to failure (ETF). For instance, UTS rose from 43.48 MPa at the lowest temperature to an impressive 245.62 MPa at the highest, a gain largely driven by enhanced atomic mobility at elevated temperatures. This increased mobility promotes better diffusion and bonding between recycled aluminum chips, resulting in a more uniform microstructure [31], [50].

Int. Journal of Integrated Engineering Vol. 17 No. 8 (2025) p. 227-243

Holding time also proves crucial for mechanical performance. Lengthier holding encourages solid solution formation and grain refinement—processes essential for strengthening the material. Both UTS and ETF improved with extended holding times, reaching peaks around 120 minutes. This underscores the need for sufficient processing time to allow key physicochemical changes, such as recrystallization and phase homogenization, to develop fully [33].

Physicochemical attributes followed similar trends. Microhardness rose by 33.66%, while density improved by 41.14%, tied to reduced porosity and microstructural refinement. These enhancements directly contribute to improved material integrity. Fracture surface examination supports these observations, revealing a shift from brittle to ductile failure modes as processing parameters increased, with higher temperatures and longer holding times producing characteristic microvoids and dimples indicative of ductile fracture [39].

A notable synergy exists between temperature and holding time: their combined effect yields greater improvements than either alone. The optimal pairing of high temperature and extended holding time maximized UTS, ETF, microhardness, and density, highlighting the importance of balancing these factors to achieve superior material performance [33], [50]

3.2 Life Cycle Assessment (LCA)

This section compared the environmental impact of recycling AA7075 aluminium chips using the DR-HPF process at the suggested optimal parameter (480°C/86 min) to the CR (remelting) process. The functional unit for both processes was 1 kg of recycling aluminium chips.

3.2.1 Life Cycle Impact Analysis (LCIA)

Figure 8 presents the endpoint categories and midpoint impact categories for different aluminum recycling routes, comparing the DR-HPF (optimal parameter) and CR (remelting) processes. The endpoint impact indicator aggregates multiple midpoint environmental stresses into three main categories: human health (HH), resources availability (RA), and ecosystem damage (ED) [51]. Both recycling routes showed the highest endpoint impact on human health, followed by resource depletion and ecosystem damage.

Using the ReCiPe method in SimaPro software, 18 midpoint impact categories were calculated, though this study focuses on the six most relevant: climate change (HH), fossil depletion (RA), particulate matter (HH), human toxicity (HH), climate change (ED), and metal depletion [11], [18]. Climate change impacts on human health were the dominant driver of endpoint impacts. Aluminum extraction and recycling processes contribute significantly to carbon dioxide emissions from fossil fuel combustion [52], [53]. The CR process emitted pollutants such as dust, smoke, nitrogen oxides, organic compounds, chlorides, and sulfur dioxides, all harmful to human health [54]. Particulate matter, a contributing factor to human health impacts, was strongly influenced by sulfur hexafluoride emissions during aluminum product manufacture. Resource depletion was dominated mainly by fossil fuel consumption—including coal, natural gas, and oil—key energy sources in aluminum production. Concerns over fossil and metal depletion have spurred the adoption of recycling technologies. Recycling aluminum offers notable environmental and economic advantages; secondary production requires only about 5% of the energy consumed in primary aluminum production [18].

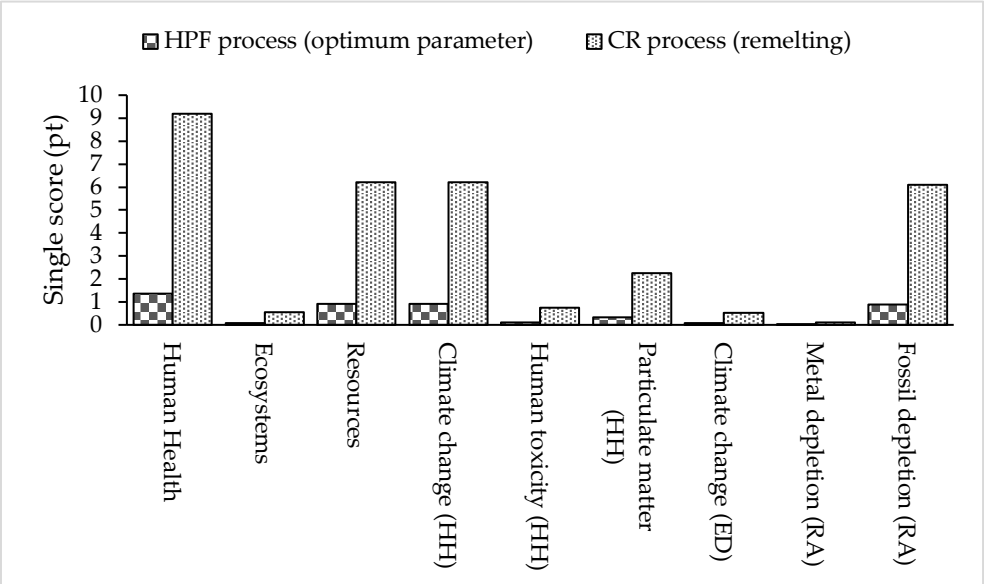

Fig. 8 *The midpoint impact categories for the HPF process (optimum parameter) and CR process routes*

Comparatively, the CR process recorded higher impact scores at both midpoint and endpoint levels than the HPF process. The CR route involves energy-intensive stages including remelting, shredding, decoating, and secondary ingot casting, resulting in low overall energy efficiency [18], [11]. A major challenge in CR is permanent metal loss through oxidation and slag formation during remelting [52], [53]. Fine chips and light scraps tend to oxidize heavily—losses can reach 15% to 20% due to their high surface area-to-volume ratio [54]. Aluminum recycling losses fall into three categories: material losses during scrap preparation, quality losses when alloy composition deviates from specifications, and dilution losses from adding high-purity metal to meet alloy standards [55], [56], [57]. Salt slag, a byproduct of remelting, is considered hazardous waste [58]. Emission of toxic gases such as ammonia, methane, hydrogen, phosphine, and hydrogen sulfide further challenges the CR approach.

Currently, CR remains the dominant remelting method in aluminum recycling plants, producing secondary ingots with controlled alloy composition. To compensate for metal losses, primary aluminum is added. Manufacturing primary aluminum from bauxite ore demands vast energy, accounting for approximately 21% of global energy use and 25% of global CO_2 emissions. Over 90% of these emissions stem from smelting and associated processes like mining, refining, and anode fabrication [59]. Variations in power generation methods throughout the supply chain greatly influence emissions inventories and environmental impacts. Indirect emissions constitute the largest share (65%), followed by process emissions (18%) and fossil fuel combustion (17%).

Emerging meltless recycling techniques aim to reduce environmental impact by applying severe plastic deformation below aluminum's solidus temperature, breaking oxide layers to enable bonding without remelting. DR-HPF provides significant environmental benefits by preventing metal losses common in remelting, where alloying elements are difficult to retain [18]. Avoiding remelting conserves energy and materials, greatly reducing the overall environmental footprint, though these meltless methods do not allow alloy composition modification. Midpoint impact categories address environmental stress types such as metal depletion, fossil depletion, particulate matter, climate change, and human toxicity. Endpoint categories translate these stresses into environmental damage across ecosystems (ED), resource availability (RA), and human health (HH), reflecting a damage-oriented approach. This methodology aligns with prior work by Llatas et al., who examined environmental impacts of recycling aluminum alloy via hot press forging [51]. Life Cycle Assessment (LCA) results for AA6061 aluminum demonstrate higher environmental burdens from CR compared to HPF processes. Comparing these findings to other aluminum recycling studies offers comprehensive insight into the varied environmental consequences of different recycling technologies, enriching our understanding of sustainable manufacturing practices.

4. Conclusion

The present study successfully optimized the direct recycling hot press forging (DR-HPF) parameters for AA7075 aluminium alloy using Response Surface Methodology (RSM), demonstrating simultaneous improvements in mechanical performance and environmental impact. The optimized conditions—480 °C forging temperature and 86 minutes soaking time—resulted in an ultimate tensile strength (UTS) of ~246 MPa, reflecting a 7.17% increase above theoretical predictions, and an elongation to failure (ETF) of 6.9%.

Life Cycle Assessment (LCA) further indicated that the optimized DR-HPF route reduces global warming potential by more than 85% and lowers energy consumption by approximately 69% compared to conventional remelting-based recycling. These findings demonstrate a unique integration of mechanical optimization with environmental assessment, affirming the meltless DR-HPF route as a sustainable and energy-efficient alternative with strong industrial relevance.

However, this study is limited by its laboratory-scale implementation and the evaluation of only two process variables. Future investigations should consider pilot-scale validation, comprehensive cost–benefit analysis, and the application of this optimization framework to additional alloy systems in order to further establish the broader applicability and commercial feasibility of the DR-HPF process.

Acknowledgement

The authors would like to express their deepest appreciation to Universiti Tun Hussein Onn Malaysia (UTHM) for the financial support provided through the Tier 1 (vot J141). Additional funding was received through the Research Enhancement-Graduate Grant (RE-GG) (vot Q203). The authors also acknowledge the Sustainable Manufacturing and Recycling Technology, Advanced Manufacturing and Material Center (SMART-AMMC), Universiti Tun Hussein Onn Malaysia for providing additional support and research facilities.

Conflict of Interest

Authors declare that there is no conflict of interest regarding the publication of the paper.

Author Contribution

The authors confirm contribution to the paper as follows: ***study conception and design****: ISTT and NKY;* ***methodology****: ISTT, NKY, MAL;* ***data collection****: ISTT;* ***software****: MHMK, MAL,* ***validation****: ISTT;* ***formal analysis and interpretation of results****: ISTT; investigation: ISTT; draft manuscript preparation: ISTT; review and editing: MHMK, SAA; visualization: MHMK; supervision: NKY; project administration: NKY; funding acquisition: NKY, SAA. All authors reviewed the results and approved the final version of the manuscript.*

References

[1] C. N. Cislo, B. Kronthaler, B. Buchmayr, and C. Weiß, "Solid state recycling of aluminum alloy chips via pulsed electric current sintering," *J. Manuf. Mater. Process.*, vol. 4, no. 1, 2020, doi: 10.3390/jmmp4010023.

[2] M. D. Vijayakumar, V. Dhinakaran, T. Sathish, G. Muthu, and P. M. B. Ram, "Experimental study of chemical composition of aluminium alloys," *Mater. Today Proc.*, vol. 37, no. Part 2, pp. 1790–1793, Jan. .

[3] K. Zhao, Y. Yang, S. N. Fedorov, and P. S. Palyanitsin, "Energy efficiency in primary aluminium industry," *IOP Conf. Ser. Mater. Sci. Eng.*, vol. 560, no. 1, p. 012180, Jun. 2019, doi: 10.1088/1757-899X/560/1/012180.

[4] T. Rivera and A. Flores, "A-242 Aluminium Alloy Foams Manufacture from the recycling of beverage cans," *Metals (Basel).*, 2019, doi: 10.3390/met9010092.

[5] S. P. Dwivedi and P. Sharma, "Utilization of waste spent alumina catalyst and agro-waste rice husk ash as reinforcement materials with scrap aluminium alloy wheel matrix," *J. Process Mech. Eng.*, 2020, doi: 10.1177/0954408920930634.

[6] D. S. Wong and P. Lavoie, "Aluminum : Recycling and Environmental Footprint," *JOM*, vol. 71, no. 9, pp. 2926–2927, 2019, doi: 10.1007/s11837-019-03656-9.

[7] A. Yasinskiy *et al.*, "Aluminium Recycling in Single- and Multiple-Capillary Laboratory Electrolysis Cells," *Metals (Basel).*, vol. 11, no. 1053, 2021.

[8] M. F. M. Nurul Farahin Mohd Joharudin, Noradila Abdul Latif, Mohammad Sukri Mustapa, Nur Azam Badarulzaman, "Effect of Burning Temperature on Rice Husk Silica as Reinforcement of Recycled Aluminium Chip AA7075," *J. Adv. Res. Fluid Mech. Therm. Sci.*, vol. 1, no. 1, pp. 125–132, 2020.

[9] K. Gancarczyk, A. Nowotnik, and G. Boczkal, "Microstructure and Properties of As-Cast and Heat-Treated 2017A Aluminium Alloy Obtained from Scrap Recycling," *Materials (Basel).*, 2021.

[10] B. Wan, W. Chen, T. Lu, F. Liu, Z. Jiang, and M. Mao, "Review of solid state recycling of aluminum chips," *Resour. Conserv. Recycl.*, vol. 125, no. June, pp. 37–47, 2017, doi: 10.1016/j.resconrec.2017.06.004.

[11] G. Buffa, D. Baffari, G. Ingarao, and L. Fratini, "Uncovering Technological and Environmental Potentials of Aluminum Alloy Scraps Recycling Through Friction Stir Consolidation," *Int. J. Precis. Eng. Manuf. - Green Technol.*, no. 0123456789, 2020, doi: 10.1007/s40684-019-00159-5.

[12] L. Hurtalová, E. Tillová, M. Chalupová, and J. Piatkowski, "Optical and Scanning Electron Microscope Studies of Recycled (Secondary) Al-Si Cast Alloys," *Solid State Phenom.*, vol. 203–204, pp. 266–271, 2013, doi: 10.4028/WWW.SCIENTIFIC.NET/SSP.203-204.266.

[13] L. Kučerová, J. Hájek, and J. Vítek, "The effect of cryogenic treatment on mechanical properties, wear and corrosion resistance of aluminium alloy AW7075," *Manuf. Technol.*, vol. 20, no. 1, pp. 60–65, 2020, doi: 10.21062/mft.2020.004.

[14] J. M. Cullen and J. M. Allwood, "Mapping the Global Flow of Aluminum: From Liquid Aluminum to End-Use Goods," *Environ. Sci. &Amp; Technol.*, vol. 47, no. 7, pp. 3057–3064, Apr. 2013, doi: 10.1021/ES304256S.

[15] A. Koch, M. Bonhage, M. Teschke, L. Luecker, B. Behrens, and F. Walther, "Electrical resistance-based fatigue assessment and capability prediction of extrudates from recycled field-assisted sintered EN AW-6082 aluminium chips," *Mater. Charact.*, vol. 169, no. September, p. 110644, 2020, doi: 10.1016/j.matchar.2020.110644.

[16] D. Baffari, G. Buffa, G. Ingarao, A. Masnata, and L. Fratini, "Aluminium sheet metal scrap recycling through friction consolidation," *Procedia Manuf.*, vol. 29, pp. 560–566, 2019, doi: 10.1016/j.promfg.2019.02.134.

[17] T. Borgert, "Analysis of Temperature Effect on Strength and Microstructure in Friction Induced Recycling Process (FIRP)," 2023. doi: 10.21741/9781644902479-211.

[18] G. Ingarao, D. Baffari, E. Bracquene, L. Fratini, and J. Duflou, "Energy demand reduction of aluminum alloys recycling through friction stir extrusion processes implementation," *Procedia Manuf.*, vol. 33, pp. 632–638, 2019, doi: 10.1016/j.promfg.2019.04.079.

[19] E. Kilickap, M. Huseyinoglu, and A. Yardimeden, "Optimization of drilling parameters on surface roughness in drilling of AISI 1045 using response surface methodology and genetic algorithm," pp. 79–88, 2011, doi: 10.1007/s00170-010-2710-7.

[20] N. Gobikannan, T. Senthilkumar, and S. Amizharasan, "Application of Response Surface Methodology and Firefly Algorithm for Optimizing Multiple Responses in Turning AISI 1045 Steel," *Arab J Sci Eng*, pp. 8015–8030, 2014, doi: 10.1007/s13369-014-1320-3.

[21] S. Daneshpayeh, F. Ashenai Ghasemi, I. Ghasemi, and M. Ayaz, "Predicting of mechanical properties of PP/LLDPE/TiO2 nano-composites by response surface methodology," *Compos. Part B Eng.*, vol. 84, pp. 109–120, 2016, doi: 10.1016/j.compositesb.2015.08.075.

[22] N. A. Rajali, S. M. Radzi, M. M. Rehan, and N. A. M. Amin, "Optimization of the Biodiesel Production via Transesterification Reaction of Palm Oil using Response Surface Methodology (RSM): A Review," *Malaysian J. Sci. Heal. Technol.*, vol. 8, no. 2, pp. 58–67, Sep. 2022, doi: 10.33102/MJOSHT.V8I2.292.

[23] U. Iqbal, V. S. Senthil Kumar, and S. Gopalakannan, "Application of Response Surface Methodology in optimizing the process parameters of Twist Extrusion process for AA6061-T6 aluminum alloy," *Meas. J. Int. Meas. Confed.*, vol. 94, pp. 126–138, 2016, doi: 10.1016/j.measurement.2016.07.085.

[24] M. A. Islam, M. R. Alam, and M. O. Hannan, "Multiresponse optimization based on statistical response surface methodology and desirability function for the production of particleboard," *Compos. Part B Eng.*, vol. 43, no. 3, pp. 861–868, 2012, doi: 10.1016/j.compositesb.2011.11.033.

[25] N. Salim, R. Hashim, O. Sulaiman, M. Ibrahim, M. Sato, and S. Hiziroglu, "Optimum manufacturing parameters for compressed lumber from oil palm (Elaeis guineensis) trunks: Respond surface approach," *Compos. Part B Eng.*, vol. 43, no. 3, pp. 988–996, 2012, doi: 10.1016/j.compositesb.2011.11.002.

[26] Y.-L. Han, J. Gao, Y.-Y. Yin, Z.-Y. Jin, X.-M. Xu, and H.-Q. Chen, "Extraction optimization by response surface methodology of mucilage polysaccharide from the peel of Opuntia dillenii haw. fruits and their physicochemical properties," *Carbohydr. Polym.*, vol. 151, pp. 381–391, 2016, doi: 10.1016/j.carbpol.2016.05.085.

[27] A. Jamekhorshid, S. M. Sadrameli, and A. R. Bahramian, "Process optimization and modeling of microencapsulated phase change material using response surface methodology," *Appl. Therm. Eng.*, vol. 70, no. 1, pp. 183–189, 2014, doi: 10.1016/j.applthermaleng.2014.05.011.

[28] I. M. Atadashi, M. K. Aroua, A. R. A. Aziz, and N. M. N. Sulaiman, "High quality biodiesel obtained through membrane technology," *J. Memb. Sci.*, vol. 421–422, pp. 154–164, 2012, doi: 10.1016/j.memsci.2012.07.006.

[29] S. N. A. S. Rahim, "Response Surface Methodology Approach to Recycling Aluminium Chips AA6061 by Optimum Hot Extrusion Parameter," *J. Eng. Sci. Res.*, vol. 3, no. 1, pp. 1–6, Feb. 2020, doi: 10.26666/RMP.JESR.2019.1.1.

[30] W. Xiao, H. Cai, W. Lu, Y. Li, K. Zheng, and Y. Wu, "Multi-objective optimization with automatic simulation for partition temperature control in aluminum hot stamping process," *Struct. Multidiscip. Optim.*, vol. 65, no. 3, Mar. 2022, doi: 10.1007/S00158-022-03190-4.

[31] N. E. Ruhaizat *et al.*, "Effect of Direct Recycling Hot Press Forging Parameters on Mechanical Properties and Surface Integrity of AA7075 Aluminum Alloys," *Metals (Basel).*, vol. 12, no. 10, 2022, doi: 10.3390/met12101555.

[32] N. K. Yusuf, M. A. Lajis, and A. Ahmad, "Life Cycle Assessment on the Direct Recycling Aluminium Alloy AA6061 Chips and Metal Matrix Composite (MMC-AlR)," *Int. J. Integr. Eng.*, vol. 13, no. 5, pp. 95–100, 2021, doi: 10.30880/ijie.2021.13.07.012.

[33] M. H. M. Khaireez *et al.*, "Life cycle assessment of direct recycling hot press forging of aluminium AA7075 metal matrix composite," *Mater. Res. Express*, vol. 11, no. 3, p. 036519, Mar. 2024, doi: 10.1088/2053-1591/ad3011.

[34] J. Green, *Aluminum recycling and processing for energy conservation and sustainability*. ASM international, Material Park, OH, 2007.

[35] D. U. Furrer and S. L. Semiatin, Eds., *Fundamentals of Modeling for Metals Processing*. ASM International, 2009. doi: 10.31399/asm.hb.v22a.9781627081962.

[36] T. S. Shih, H. T. Hsu, and L. R. Hwang, "Factors affecting the microstructure, tensile properties and corrosion resistance of aa7075 forgings," *Materials (Basel).*, vol. 14, no. 19, 2021, doi: 10.3390/ma14195776.

[37] Y. L. Chang, F. Y. Hung, and T. S. Lui, "A new infrared heat treatment on hot forging 7075 aluminum alloy: Microstructure and mechanical properties," *Materials (Basel).*, vol. 13, no. 5, 2020, doi: 10.3390/ma13051177.

[38] I. SAE, "Aerospace Material Specification: Heat Treatment of Wrought Aluminum Alloy Parts," SAE International, 400 Commonwealth Drive, Warrendale, PA, United States, Aug. 2006. doi: 10.4271/AMS2770R.

[39] D. C. Montgomery, *Design and analysis of experiments*. New York: Wiley, 2016. doi: 10.2307/2983009.

[40] S. S. A. Amr, H. A. Aziz, and M. J. K. Bashir, "Application of Response Surface Methodology (RSM) for Optimization of Semi-Aerobic Landfill Leachate Treatment Using Ozone," *Appl. Water Sci.*, vol. 4, no. 3, pp. 231–239, 2014, doi: 10.1007/s13201-014-0156-z.

[41] A. Ahmad and B. H. Hameed, "Effect of Preparation Conditions of Activated Carbon From Bamboo Waste for Real Textile Wastewater," *J. Hazard. Mater.*, vol. 173, no. 1–3, pp. 487–493, 2010, doi: 10.1016/j.jhazmat.2009.08.111.

[42] A. K. Swarnakar, P. P. Srivastav, and S. K. Das, "Optimization of Pressure Parboiling Conditions and Pre-Conditioned Moisture Content of Brown Rice (Unpolished Rice) for Microwave Puffing and Its Comparison With Hot Sand Bed Puffing," *Int. J. Food Stud.*, vol. 9, 2020, doi: 10.7455/ijfs/9.si.2020.a1.

[43] N. González-Silva *et al.*, "Ultrasound-Assisted Extraction of Phenolic Compounds from Psidium cattleianum Leaves: Optimization Using the Response Surface Methodology," 2022. doi: 10.3390/molecules27113557.

[44] G. Derringer and R. Suich, "Simultaneous optimization of several response variables," *J. Qual. Technol.*, vol. 12, no. 4, pp. 214–219, 1980.

[45] L. cycle assessment. Technical Committee ISO/TC 207, Environmental management, Subcommittee SC 5, "ISO 14040:2006 Environmental management — Life cycle assessment — Principles and framework," vol. 1997, 2006.

[46] I. Standard, T. S. Preview, and The International organization for standardization, "ISO 14044 Environmental management-Life cycle assessment-Requirements and guidelines Management environnemental-Analyse du cycle de vie-Exigences et lignes directrices iTeh STANDARD PREVIEW," *Int. Organ. Stand.*, vol. 2006, p. 7, 1404.

[47] M. A. J. Huijbregts *et al.*, "ReCiPe2016: a harmonised life cycle impact assessment method at midpoint and endpoint level," *Int. J. Life Cycle Assess.*, vol. 22, no. 2, pp. 138–147, Feb. 2017, doi: 10.1007/S11367-016-1246-Y.

[48] L. Johnson, "How to Calculate 3 Phase Power | Sciencing."

[49] H. W. Beaty and S. Santoso, *Handbook of electric power calculations*. New York: MCGRAW-HILL, 2015.

[50] N. K. Yusuf, A. S. Medi, M. A. Lajis, B. L. Chan, and S. Shamsudin, "Mechanical Properties of Direct Recycling Metal Matrix Composite (MMC-AlR) AA7075 Aircraft Aluminium Alloy," *Int. J. Integr. Eng.*, vol. 13, no. 7, pp. 89–94, 2021, doi: 10.30880/ijie.2021.13.07.011.

[51] C. Llatas, R. Quiñones, and N. Bizcocho, "Environmental Impact Assessment of Construction Waste Recycling versus Disposal Scenarios Using an LCA-BIM Tool during the Design Stage," *Recycling*, vol. 7, no. 6, Dec. 2022, doi: 10.3390/RECYCLING7060082.

[52] D. Paraskevas, K. Kellens, W. Dewulf, and J. R. Duflou, "Environmental modelling of aluminium recycling: a Life Cycle Assessment tool for sustainable metal management," *J. Clean. Prod.*, 2014, doi: 10.1016/j.jclepro.2014.09.102.

[53] L. Wang, "Life Cycle Assessment (LCA) and Eco-Profile of Plastic, Glass, and Aluminium Bottles," *EngRN Ind. Ecol.*, Sep. 2020, doi: 10.2139/SSRN.3679112.

[54] Y. Xiao and M. A. Reuter, "Recycling of distributed aluminium turning scrap," *Miner. Eng.*, vol. 15, no. 11 SUPPL. 1, pp. 963–970, 2002, doi: 10.1016/S0892-6875(02)00137-1.

[55] H. M. Amini, A. Moloodi, M. Golestanipour, and E. Z. V Karimi, "Recycling of aluminium alloy turning scrap via cold pressing and melting with salt flux," *J. Mater. Process. Technol.*, vol. 209, no. 7, pp. 3138–3142, Apr. 2009, doi: 10.1016/j.jmatprotec.2008.07.020.

[56] M. B. G. Castro, J. A. M. Remmerswaal, M. A. Reuter, and U. J. M. Boin, "A thermodynamic approach to the compatibility of materials combinations for recycling," *Resour. Conserv. Recycl.*, vol. 43, no. 1, pp. 1–19, 2004, doi: 10.1016/j.resconrec.2004.04.011.

[57] R. Chiba, T. Nakamura, and M. Kuroda, "Solid-state recycling of aluminium alloy swarf through cold profile extrusion and cold rolling," *J. Mater. Process. Technol.*, vol. 211, no. 11, pp. 1878–1887, 2011, doi: 10.1016/j.jmatprotec.2011.06.010.

[58] D. Brough and H. Jouhara, "The aluminium industry : A review on state-of-the-art technologies , environmental impacts and possibilities for waste heat recovery," *Int. J. thermofluids*, vol. 2, 2020, doi: 10.1016/j.ijft.2019.100007.

[59] D. Paraskevas, K. Kellens, A. Van de Voorde, W. Dewulf, and J. R. Duflou, "Environmental Impact Analysis of Primary Aluminium Production at Country Level," *Procedia CIRP*, vol. 40, pp. 209–213, 2016, doi: 10.1016/j.procir.2016.01.104.